

Radiative strength functions from the energy-localized Brink-Axel hypothesis

Oliver C. Gorton,* Konstantinos Kravvaris, and Jutta E. Escher

Lawrence Livermore National Laboratory, P.O. Box 808, L-414, Livermore, California 94551, USA

Calvin W. Johnson

San Diego State University, San Diego, California 92182, USA

Radiative strength functions (RSFs) model the bulk electromagnetic response of highly-excited nuclei and are critical inputs for statistical reaction codes. In this paper, we present a definition of the RSF that is consistent with Hauser-Feshbach reaction codes and that can be efficiently computed with the shell model using the Lanczos strength-function (LSF) method. We introduce a variant of the shell model LSF method that exploits the energy-localized Brink-Axel hypothesis, which makes it possible to compute both electric and magnetic RSFs across all energies relevant to capture reactions. We verify agreement with the conventional definition of RSFs with benchmark calculations of ^{24}Mg , then present novel results for ^{56}Fe . For ^{56}Fe we find that: (i) the M1 RSF shape evolves smoothly with excitation energy, consistent with the energy-localized Brink-Axel hypothesis, (ii) both M1 and E1 transitions contribute significantly to the radiative strength below the photo-absorption threshold, and (iii) within the $sdpf$ model space, the strength below 3 MeV observed in Oslo-type experiments cannot be fully reproduced. These results pave the way for a coherent microscopic description of RSFs and further motivate the use of energy-dependent RSFs in modern reaction codes.

I. INTRODUCTION

In 1952, Blatt and Weisskopf [1] commented “an exact theoretical description of [radiative transitions to or from highly excited levels] is impossible, since the radiative transition probabilities can be calculated only if the nuclear wave functions are known”. Today, this statement continues to represent a compelling challenge since models for radiative decay are an essential ingredient in the Hauser-Feshbach (HF) reaction codes [2–6] that underpin many applications in basic science [7–9] and nuclear technology [10, 11]. Many theoretical and experimental efforts have sought to understand how to approximate radiative decay [12–16], resulting in phenomenological models called gamma (photon) strength functions [14]. We prefer the nomenclature *radiative* strength functions (RSFs) to align with the specific form used in HF theory.

From an experimental standpoint, RSFs are notoriously difficult to measure unambiguously across a wide energy range, especially for radioactive isotopes [17–20]. Thus, the first RSF models approximated the photo-emission probability using the photo-absorption cross section of nuclear ground states [12], which can be measured in a more straightforward manner [21]. However, this approximation runs afoul of neutron capture data which predicts nonzero strength below the photo-absorption energy threshold. Low-energy photons are attributable to the exponential growth of transitions available to highly excited nuclei [22, 23] and models have long included temperature-dependent corrections to account for these effects [14, 16, 24]. Because this energy regime plays a crucial role in neutron-capture reactions

during nucleosynthesis [7, 8], there have been significant efforts to understand the low-energy behavior of these functions [22, 25–34]. However, the most common experimental method cannot probe transitions below a few MeV [18].

With advancements in many-body methods and computing hardware, there are now practical methods for computing accurate nuclear wave functions from microscopic models, enabling RSFs to be calculated and tabulated. While mean-field methods like Hartree-Fock Bogoliubov (HFB) coupled with the quasiparticle random-phase approximation (QRPA) have been broadly successful for this task [35–39], the low-energy predictions of these models are currently supplemented with empirical correction factors informed by shell-model calculations [35]. Although, recent work has shown it is possible to overcome this limitation [38].

Calculation of low-energy magnetic RSFs using the large-scale shell model (LSSM) is now commonplace [19, 22, 23, 26, 28, 30–32, 40], and some calculations even include electric contributions (which require larger model spaces) [28, 41, 42]. LSSM calculations have been instrumental to interpret the enhanced strength, typically referred to as the low-energy enhancement (LEE) [19, 26, 43], observed using the Oslo method [44, 45]. However, a LSSM-only description remains impractical due to computational costs driven by a) the apparent need to calculate thousands of individual wave functions to capture the LEE, and b) the extended model spaces required for the highly collective and cross-shell electric transitions.

Now that it is possible to predict the radiative decay of highly excited nuclei from microscopic models, a new challenge arises: to predict RSFs across a wide range of energies within a single framework while also building the underlying nuclear wave functions from realistic nuclear interactions and accurate many-body methods. We

* gorton3@llnl.gov

address this challenge by demonstrating that RSFs, including the LEE, can be computed using the Lanczos strength-function method (section III), so long as the Lanczos pivot vector is constructed from an excited state wave function. This approach becomes apparent only after we clarify the relationship between traditional sum-rule strength functions and the RSFs used in statistical reaction theory (section II). Using this new approach, we explore the RSF of ^{56}Fe and show that (i) the magnetic dipole RSF shape evolves with excitation energy, consistent with an energy-localized Brink-Axel hypothesis, (ii) electric dipoles transitions contribute significantly to the low-energy radiative strength, and (iii) within the $sdpf$ model space, the LEE observed in Oslo-type experiments cannot be fully reproduced below 3 MeV (section IV).

II. THEORY

In this section, we review the multiple definitions of RSFs in the literature. Then, we present a simplified definition which is compatible with HF conventions while enabling a new computational technique.

A. Preliminaries

In HF theory [46], the probability that an excited state of the compound nucleus will decay with a photon of energy E_γ is proportional to the so-called transmission coefficient $T^{XL}(E_\gamma)$, with X denoting the electromagnetic character of the transition ($X = M$ for magnetic and $X = E$ for electric) and L denoting the multipolarity of the transition. The transmission coefficient is in turn proportional to the *radiative strength function* (RSF; denoted $f(E_\gamma)$) which is the energy-averaged radiative decay width, rescaled by a phase-space factor of the photon energy E_γ [1]:

$$T^{XL}(E_\gamma) = 2\pi E_\gamma^{2L+1} \overleftarrow{f}^{XL}(E_\gamma). \quad (1)$$

Here $E_\gamma = E_i - E_f$ is the transition energy between an initial level i with energy E_i and a final level f with energy E_f . The arrow \leftarrow indicates “downward” strength ($E_i > E_f$). As written in Eq. (1), the RSF depends only on XL and E_γ . In a many-body microscopic theory, however, other dependencies such as the structure and quantum numbers of the initial and final levels may apply.

The standard definition of RSFs in terms of nuclear structure quantities was given by Bartholomew in 1973 [47]. As restated by Kopecký and Tomandl [48], the Bartholomew definition of the RSF is the product of an average decay width and a level-density-like quantity:

$$\overleftarrow{f}_{\text{Barth.}}^{XL}(E_\gamma) = \frac{1}{E_\gamma^{2L+1}} \langle \Gamma_{fi}^{XL} \rangle_i \rho(E_i, j_i). \quad (2)$$

Here, $\langle \Gamma_{fi}^{XL} \rangle_i$ is the average partial decay width between initial levels i and a single final level f , for transitions of

multipole type XL . The average is over all initial levels i near E_i leading to transitions with energy E_γ (and conserving angular momentum). $\rho(E_i, j_i)$ is the density of levels near E_i with spin j_i which can decay to f .

The partial decay width for the level i can be written in terms of reduced transition probabilities (B -values):

$$\Gamma_{f \leftarrow i}^{XL} = \frac{8\pi(L+1)}{L[(2L+1)!!]^2} k_\gamma^{2L+1} B_{f \leftarrow i}^{XL}, \quad (3)$$

where $k_\gamma = E_\gamma/(\hbar c)$, and $B_{f \leftarrow i}^{XL}$ directly relates to nuclear wave functions and transition operators:

$$B_{f \leftarrow i}^{XL} = \frac{1}{2j_i + 1} |\langle \psi_f | \mathcal{M}^{XL} | \psi_i \rangle|^2. \quad (4)$$

The nuclear wave functions $|\psi_x\rangle$ have energy E_x , total angular momentum-parity $j_x^{\pi_x}$, and magnetic substates m_x . The B -values are reduced matrix elements (indicated by the double bar), meaning the final state magnetic quantum numbers (m_f) have been summed and the initial substates (m_i) averaged [49]. Matrix elements for the multipole operator \mathcal{M}^{XL} can be found in standard texts [1, 50, 51].

The contemporary method for computing RSFs with the LSSM was first established by Schwengner *et al.* [22] and made explicit by Brown and Larsen [26]. Inserting Eq. (3) into Eq. (2), one can write down a special form of Eq. (2) for magnetic dipole transitions [19, 22, 26, 32, 43]:

$$\overleftarrow{f}_{\text{Barth.}}^{\text{M1}} = \frac{16\pi}{9(\hbar c)^3} [B_{f \leftarrow i}^{\text{M1}}]_{fi}(E_i, j_i^{\pi_i}, E_\gamma) \rho(E_i, j_i^{\pi_i}), \quad (5)$$

where $[\cdot]_{fi}$ is the “pixel-average”: all non-zero B -values are sorted into $(100 \text{ keV})^2$ “pixels”, with E_i along one axis and E_γ along the other, then divided by the number of B -values in each pixel [26]. Finally, Eq. (5) is averaged over $j_i^{\pi_i}$ and E_i when plotted as a function of E_γ [31, 32]. For the remainder of the paper we omit π_x labels, since for a given XL transition only a single value is allowed.

The details of the level density’s spin and parity dependence in Eq. (5) has produced some confusion, as explained in the appendix of Ref. [31]. If we define RSFs primarily in terms of discrete transition probabilities (the natural language of the shell model), without reference to level densities, these issues disappear.

When dealing with discrete transition probabilities, one typically works with *sum-rule strength functions* of the form [52–54]:

$$S^{XL}(E_i, E_\gamma) = \sum_f \delta(E_f - E_i + E_\gamma) B_{f \leftarrow i}^{XL}, \quad (6)$$

which do not explicitly refer to level densities. While Eq. (6) is directly proportional to the photo-absorption cross section when $E_i = 0$ (and $E_f > E_i$), it is incompatible with the conventions of HF theory (see Appendix A). Thus, in order to reconcile the two, we present a level-density-free (LDF) definition of the RSF which also simplifies the algorithm for computing RSFs within the LSSM framework.

B. Level-density-free definition

HF theory expresses all cross sections in the language of *decay* widths, regardless of whether a given nuclear state is absorbing or emitting radiation. We therefore find it useful to replace the notation of “initial levels” i and “final levels” f . Instead, we define “compound-nucleus (CN) levels” c and “de-excited levels” d to imply $E_c > E_d$, as shown in Fig. 1.

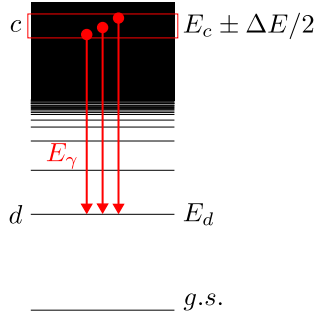


FIG. 1. Depiction of the radiative strength function, Eq. (10). The red arrows indicate partial decay widths from levels $c \rightarrow d$; the box indicates an energy-average over partial decay widths from within $E_c \pm \Delta E/2$.

Consider a nuclear level d impinged upon by an unpolarized beam of photons with energy E_γ . The energy-averaged cross section for this level to be excited to an energy near $E_c = E_d + E_\gamma$ is (c.f. Ref [55] p.324):

$$\langle \sigma_\gamma^{XL} \rangle(E_\gamma) = \frac{\pi}{k_\gamma^2} \sum_{j_c} \frac{(2j_c + 1)}{w(s)(2j_d + 1)} T_{d,j_c}^{XL}(E_\gamma), \quad (7)$$

which includes a sum over the spins j_c of the CN levels, where $j_c = j_d + \mathbf{L}$ (i.e., all spins allowed by angular momentum coupling). $T_{d,j_c}^{XL}(E_\gamma)$ are the photon transmission coefficients, $w(s) = 2$ is the statistical factor for incoming photons, and the remaining statistical factors account for the fact that $T_{d,j_c}^{XL}(E_\gamma)$ describe *decay* probabilities for $c \rightarrow d$, even though Eq. (7) describes a physical process for $d \rightarrow c$. By convention, transmission coefficients always refer to particle *emission* (in this case, photons).

The transmission coefficients are related by Eq. (1) and the Bartholomew definition Eq. (2) to the energy-averaged partial decay widths for $c \rightarrow d$ [1, 13, 47]:

$$T_{d,j_c}^{XL}(E_\gamma) = 2\pi \langle \Gamma_{d \leftarrow c}^{XL} \rangle_c \rho(E_c, j_c). \quad (8)$$

At this point we can remove an approximation implicit in this expression. It can be shown that Eq. (8) can equally be written as an energy-average, rather than the product of an average and a level density (c.f. Blatt and

Weisskopf [1], p.653):

$$\begin{aligned} T_{d,j_c}^{XL}(E_\gamma) &= 2\pi \left(\frac{1}{N_c} \sum_{c'} \delta_{j_c' j_c} \Gamma_{d \leftarrow c'}^{XL}(E_\gamma) \right) \left(\frac{N_c}{\Delta E} \right) \\ &= 2\pi \frac{1}{\Delta E} \sum_{c'} \delta_{j_c' j_c} \Gamma_{d \leftarrow c'}^{XL}(E_\gamma), \end{aligned} \quad (9)$$

where $N_c = N_c(E_c, j_c)$ is the number of partial widths included in the sum (the same number as in the average). Eq. (8) is an approximation of Eq. (9) because the number of compound levels which contribute to the average, N_c , depends on the specific de-excited level d and is merely bounded by the level density: $N_c/\Delta E \leq \rho(E_c, j_c)$. While this approximation is effective (see section III A), we favor Eq. (9) because it depends only on partial widths, the natural language of the shell model, and enables the efficient computational techniques that we introduce in section III.

Finally, we combine Eq. (1) with Eq. (9) to obtain the main result of this section, a level-density-free (LDF) definition of the radiative strength function:

$$f_{d,j_c}^{XL}(E_\gamma) = \frac{1}{E_\gamma^{2L+1}} \frac{1}{\Delta E} \sum_{c'} \delta_{j_c' j_c} \Gamma_{d \leftarrow c'}^{XL}, \quad (10)$$

where we omit the arrow \leftarrow since from here on we deal exclusively with radiative strengths for which $E_c > E_d$ is implied (as in Fig. 1). In this form, the RSF appears as the “ E_γ -gated” total decay width to a de-excited level d from levels with angular momentum j_c . A key detail of Eq. (10) is that, regardless of whether the RSF is used to compute photo-absorption or radiative decay, the sum over decay widths $\Gamma_{d \leftarrow c}$ always runs over CN levels c . This detail not only sets the correct statistical factors in the B -values (i.e. $1/(2j_c + 1)$), but it also determines which level density the RSF is proportional to ($\rho(E_c)$, not $\rho(E_d)$). In Appendix A, we show the consistency of this convention in relation to different concepts: capture cross sections in terms of B -values, generalized transmission coefficients for radiative decay, and sum-rule strength functions.

In a microscopic theory, $f_{d,j_c}^{XL}(E_\gamma)$ may depend on the de-excited level d and the spin j_c . In HF theory, however, RSFs are generally assumed to be independent of both of these quantities. Reducing Eq. (10) to a spin-independent form is done with a simple average:

$$f_d^{XL}(E_\gamma) = \langle f_{d,j_c}^{XL}(E_\gamma) \rangle_{j_c} \quad (11)$$

$$= \frac{1}{n_{j_c}} \sum_{j_c} f_{d,j_c}^{XL}(E_\gamma), \quad (12)$$

where n_{j_c} is the number of j_c allowed by angular momentum rules. Furthermore, the strong Brink-Axel hypothesis holds that the RSF should be independent of d . Historically, this hypothesis was used to justify using the RSF of the ground state, $f_{d=1}^{XL}(E_\gamma)$ ($E_{d=1} = 0$), as the RSF for decays to any other level [12, 13]. However, it

has been shown that the strong hypothesis is not supported from a microscopic perspective, and at most one should assume the energy-localized Brink-Axel (ELBA) hypothesis [54, 56].

The work following Schwengner *et al.* [22] has already taken the first step to reject the strong Brink-Axel hypothesis, since it explicitly includes radiative strength to excited states; this move is what led to the discovery that the LSSM could reproduce the LEE (see Eq. (5) discussion). In our formalism, the equivalent energy- and spin-independent RSF is:

$$f_{(SA)}^{XL}(E_\gamma) = \langle f_{d,j_c}^{XL}(E_\gamma) \rangle_{d,j_c}, \quad (13)$$

where the average is first over j_c and second over d . Eq. (13) can therefore be directly compared to the averaged version of Eq. (5). In this paper, we take the next step towards RSFs that reflect the ELBA hypothesis.

To summarize, the LDF-RSF should be interpreted as the energy-averaged radiative strength to a specific nuclear level d , and the same form applies for HF calculations of both photo-absorption and radiative decay. As discussed in the next section, the LDF-RSF formulation allows us to use the Lanczos strength function method to compute it.

III. METHOD DEVELOPMENT

In this section, we propose a new approach for computing RSFs that mirrors the ELBA hypothesis and uses the Lanczos methods [57–59] developed for sum-rule strength functions. In section III A, we validate our LDF-RSF, Eq. (10), using LSSM calculations of ^{24}Mg in the sd valence space, for which thousands of converged wavefunctions can be obtained. Then, in section III B, we show that the low-energy behavior of the RSF emerges as a result of the excitation energy of the de-excited level, rather than the mere fact of including many transitions among excited states. Finally, in section III C, we suggest an efficient approximation scheme for radiative strength functions (RSFs) using the existing Lanczos strength function method (LSF), which avoids the need to compute transitions between many excited states.

A. Tests in the sd -shell

We find that our new LDF-RSF formula (10) agrees overall with the Bartholomew prescription of Eq. (2), although there are small deviations, due to binning effects (see Fig. 2). In the Bartholomew formula as implemented with pixel-based averaging, strengths are first simultaneously averaged over both CN levels c and de-excited levels d , then multiplied by the level density $\rho(E_c, j_c)$. This second step approximately “undoes” the first average over CN levels c . As a result, information is lost about the number of levels c with nonzero transition strengths to

particular levels d , and it is assumed that this number is given by $\rho(E_c, j_c)$ for all d . For the largest E_γ values corresponding to transitions to low-lying states, the level density $\rho(E_c, j_c)$ tends to over-predict the actual number of nonzero transitions, since not all levels c connect to all de-excited levels d . Our formulation of Eq. (10) avoids this unnecessary approximation.

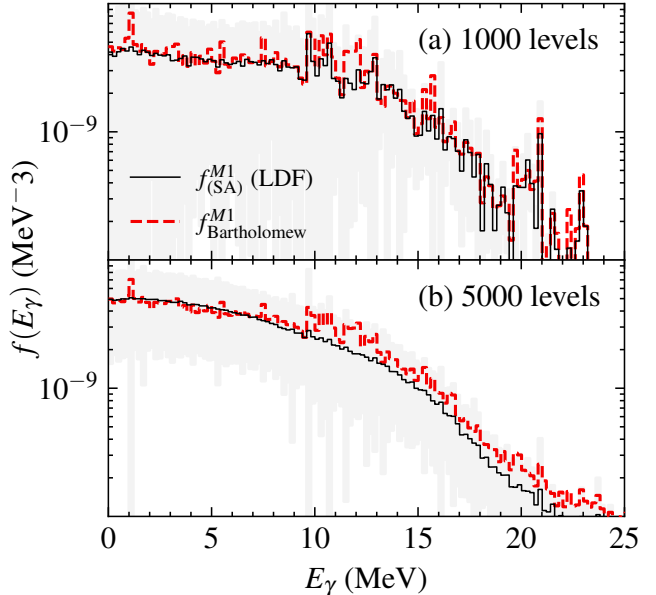


FIG. 2. Agreement of the Bartholomew formula (dashed) and the present level-density-free (LDF) formula (solid), demonstrated for the M1 RSF of ^{24}Mg . Panel a) was computed using the first 1000 levels and panel b) with the first 5000 levels (see text for details). All calculations used a bin size $\Delta E = 200$ keV. The gray band shows the standard deviation of the RSFs f_d within each bin, which are averaged to obtain $f_{(SA)}^{XL}$.

To perform the two RSF calculations in each panel of Fig. 2, we used the same set of LSSM $B(\text{M1})$ -values computed for ^{24}Mg . We used the sd model space and the USDB [60] effective interaction, which we diagonalized with the BIGSTICK shell model code [61]. We used the standard one-body M1 operator with coupling constants $g_l^p = 1$, $g_l^n = 0$, $g_s = 5.5857$, and $g_s^n = -3.8263$. In study (a), we use the lowest 1000 states of ^{24}Mg which generates $180 \cdot 10^3$ nonzero $M1$ transitions with $E_d < E_c$. In study (b), we use the 5000 lowest states of ^{24}Mg which generates $4 \cdot 10^6$ transitions. Both (a) and (b) are plotted with a bin size of $\Delta E = 200$ keV.

In addition to the averaged strength (which in the final step averages f_d over all de-excited levels d), we also present the standard deviation of f_d within each bin. The gray bands in Fig. 2 show the $+1$ and -1 standard deviations about the mean $\langle f_d \rangle$. This band does not necessarily correspond to an uncertainty, but rather it shows the variability of the radiative strength functions from one de-excited state to another (for one thing, the dis-

tribution of strengths is not normal, but closer to a χ^2 distribution). The size of the band is therefore related to the concept of Porter-Thomas fluctuations of the radiative strengths [62–64]: since the partial widths follow a χ^2 distribution, the mean tends to fluctuate over a broad range until a sufficient number of terms are summed (the bands also therefore depend on the size of the bins).

As a consequence, as we increase the number of states in the average (either by increasing the number of levels in the calculation or increasing the bin size), this standard deviation decreases. In the HF framework, the applicability of radiative strength functions relies on the level density near the de-excited state $\rho(E_d, j_d)$ being sufficiently high such that the Porter-Thomas fluctuations are sufficiently small.

B. Energy-localized Brink-Axel hypothesis

We can now demonstrate that the shape of the RSF evolves with the energy of the de-excited level d on which the RSF is built. While the ELBA hypothesis holds that the total strength of a transition operator evolves smoothly with the energy of d [54], we further show that is it primarily the low-energy strength (i.e. below the photo-absorption threshold) that increases with the energy of the de-excited level.

Using Eq. (10), it is trivial to decompose the LDF-RSF into contributions from individual de-excited levels d . We do so for the ground state $d = 1$ and a highly excited state $d = 239$. For the RSFs to specific de-excited states f_d , we take the additional step of folding with a Lorentzian of width $\Gamma = 1$ MeV in order to smooth the visual representation, as is sometimes done to approximately account for missing collectivity at higher energies [53] and effects due to the continuum [65] (see Fig. 3).

For the ground state, there is no strength below $E_\gamma = 4$ MeV, since the lowest 1^+ state is predicted around this energy; we call this the photo-absorption threshold. Overall, the shape of this RSF could be approximated by a single Lorentzian function centered around 10 MeV, which is the standard form for the M1 RSF in HF codes [66].

For the highly-excited level near $E_d = 17.05$ MeV ($d = 239$), however, maximum strength occurs below 1 MeV. Notably, the sudden drop in the strength above 16 MeV in this case is not physical, but reflects the limited number of levels computed in this example: of the 5000 states the maximum excitation energy is 33 MeV; with $E_d = 17$ MeV, the maximum $E_\gamma = 33 - 17 = 16$ MeV. A scan across all levels from $d = 1$ to $d = 239$ (not shown) shows a gradual saturation of the M1 strength at low energies. The behavior exemplified by the $d = 239$ level appears to be typical for highly-excited levels, and comparison to the mean further suggests this is the norm.

The area under the two curves in Fig. 3 approximately reveals what has already been explored by Johnson [54], which is that the integrated strength functions (propor-

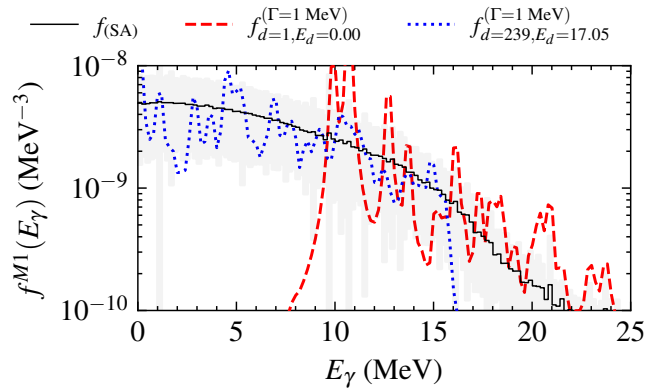


FIG. 3. Contribution of two individual strength functions $f_d^{M1}(E_\gamma)$ to the overall reduced strength $f_{(SA)}^{XL}(E_\gamma)$, showing that the ground state has a unique shape, while a random excited state has a partial radiative strength function with a shape compatible with the total reduced radiative strength function. The ground state ($d = 1$) has no strength below about 7 MeV due to a physical lack of states close enough in energy. The $d = 239$ strength, on the other hand, has significant strength approaching $E_\gamma = 0$.

tional to sum rules) violate the strong Brink-Axel hypothesis. The M1 strength function built on the ground state has overall smaller strength than that of the excited states. As a result, the RSF built on the ground state is not representative of the average decay strength. At first, this difference in total strength suggests one is doomed to compute thousands of wave functions and millions of transition probabilities whenever one wants to compute the RSFs relevant for capture reactions (which always involved highly-excited nuclei). However, there are two key points that mitigate this conclusion:

(i) Johnson [54] and Herrera *et al.* [56] showed that the total (sum-rule) strength of a level varies smoothly with the energy of that level, leading to the ELBA hypothesis. The maximum range of this total strength varies by a factor of 5-6 for M1 isovector and E2 isoscalar responses, but much less for E1 response, which in part explains the success of the strong Brink-Axel hypothesis for E1 strengths. Therefore, if we are interested in the strength for levels in a certain energy range, it is reasonable to expect that an energy-localized average should be representative. It is also known that accurate strength functions for individual levels can be obtained using approximate wave functions using the Lanczos strength-function method [57–59], again due to the ELBA hypothesis [56, 67],

(ii) The present results suggest that RSFs built on a single level d (which are closely related to the energy-distribution of the total sum-rule) tend to follow a predictable trend, so long as E_d is in a region where the level spacing is small compared to the E_γ of interest. In other words, the RSFs built on low-lying states seem to be the exception to a more universal trend. This observation suggests we can learn a general low-energy behavior of

the RSF from a small number of excited states.

In the next subsection, we leverage these two considerations to introduce a new scheme to compute RSFs.

C. Lanczos strength function method

Inspired by the ELBA hypothesis, we seek to approximate the RSF at low-energies using a small number of individual levels d positioned several MeV above the ground state. The ELBA hypothesis suggests that the strength function should vary slowly for levels nearby in energy. By averaging the individual strength functions of a small number of nearby excited states, we should be able to approximate the average RSF.

Additionally, there are well established methods to rapidly compute sum-rule strength functions for a single level, namely, the Lanczos strength function method (LSF). The LSF method approximates the strength function of a single level using a modified Lanczos algorithm [57–59]. Each iteration of the LSF method essentially resolves a new moment of the strength distribution, rather than generating one transition probability at a time. In this subsection, we demonstrate the effectiveness of this method to approximate RSFs for a single level d . Here we highlight: (i) a key difference from sum-rule strength function methods is that we sum only radiative strengths ($E_c > E_d$), and (ii) we assume spin-independence of the strength in order to simplify calculation of the matrix elements. We give further details of our LSF implementation in Appendix B.

The LSF method can approximate the RSF for individual de-excited levels d . We show an example in Fig. 4. In this case, we generated excited wave functions (interior eigenstates) using thick-restart block Lanczos [68], as done by Herrera *et al.* [56]. Additionally, we specifically targeted pivot states with $j_d = 0$ in order to simplify the strength function calculation, as discussed in Appendix B. We then applied the M1 operator and performed 200 Lanczos iterations on the pivot to obtain the reduced matrix elements for the strength function calculation. We label this scheme the *interior-eigenstate Lanczos strength-function* (ILSF) method.

The error of the LSF method relative to the exact calculation is negligible below the energies where states are available for the exact calculation ($E_{\max} - E_d \approx 33 - 17 = 16$ MeV). Above this energy, where the exact method fails, the LSF method provides results closely following the trend of the average strength, $f_{(SA)}^{XL}$.

The LSF method by itself approximates only the strength function for a single level, f_d^{XL} , and yields fine structures unique to the pivot level d . To approximate the average radiative strength function, we average over five nearby $j_d = 0$ levels (obtained with an interior eigenstate method). The result is shown in Fig. 5.

While the averaged ILSF result still contains local structures from its constituent individual strength functions, we have significantly reduced the computational

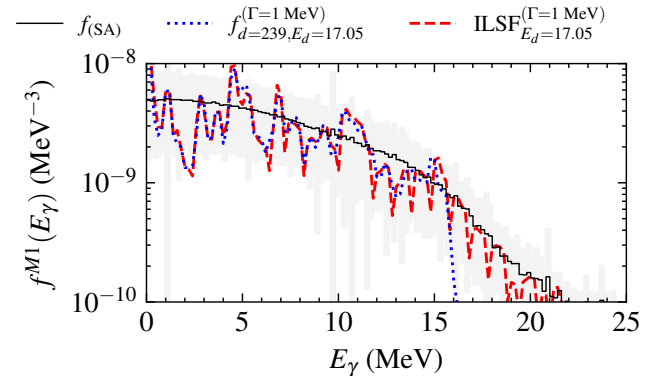


FIG. 4. The radiative strength function for a single state can be computed accurately and to higher energy with the LSF method. We demonstrate with a level with $E_d = 17.05$ near the neutron separation energy $S_n(^{24}\text{Mg}) = 16.531$ MeV. We compare the result from the complete list of transitions against that from the ILSF method (see text). The state was selected to have $j_d = 0$ so that Eq. (B5) applies, simplifying the calculation.

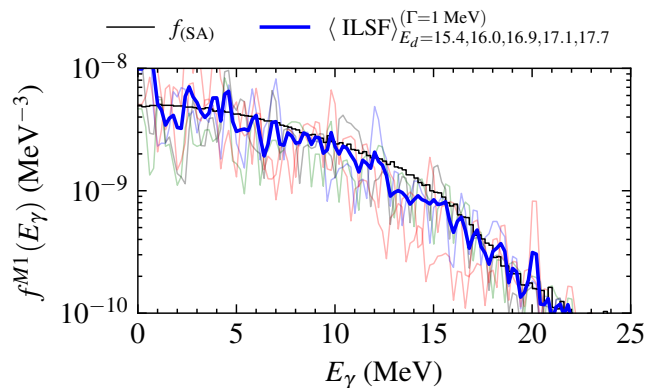


FIG. 5. The Lanczos strength-function method with interior eigenvalues (ILSF) can be further improved by averaging the partial strength functions of several approximate excited levels. Here we use five $j_d = 0$ interior eigenvectors with energies between 15 and 18 MeV as pivots. The fluctuations of individual strengths averages out to closely follow the average RSF $f_{(SA)}^{M1}$ computed with 5000 levels.

cost compared to the full calculation: converging the 5000 levels used in the full $f_{(SA)}^{XL}$ required more than 18000 Lanczos iterations (one *iteration* is essentially one matrix-vector multiplication). By contrast, for the ILSF method, approximate convergence of 5 interior wave functions required only 80 block iterations, followed by 200 iterations for each level to compute the strength distributions. In total, ILSF used about 1400 iterations, reducing the cost by more than ten-fold. Furthermore, by not having to store multiple vectors in memory/disk, the ILSF approach scales significantly better in larger systems.

IV. RESULTS FOR IRON

We now turn to the computationally demanding ^{56}Fe nucleus, for which existing shell model methods to compute the E1 RSF up to energies relevant for radiative capture calculations would be impractical.

From an experimental standpoint, ^{56}Fe was one of the first nuclei observed to have a low-energy enhancement (LEE) of the RSF. The ^{56}Fe LEE has been observed in ^3He scattering by Voinov *et al.* [69] (Fig. 7: red dots) and Algin *et al.* [70] (blue triangles), and $(p, p'\gamma)$ scattering by Larsen *et al.* [71] (black squares), along with the proton inelastic scattering data from Jingo *et al.* [72] (green crosses). However, there is currently no microscopic model that can reproduce the magnitude of strength measured below 3 MeV. LSSM calculations indicate M1 transitions are not the source of the surplus strength [26, 31], and so far it has been impractical to compute the low-energy E1 strength with the LSSM. Adding to the tension between different approaches, a re-analysis of decay widths from neutron-resonance data suggested significantly weaker LEE [48], and Kopecký and Tomandl [48] argued that the scattering experiments should be revisited.

In this section, we compare to the systematic model calculations of Goriely *et al.* [35, 73], so we summarize the relevant points from their work. The calculations of [35] begin with axially symmetric deformed quasiparticle random-phase approximation (QRPA) based on the finite-range D1M Gogny force (to be denoted as “D1M+QRPA”). The E1 and M1 strengths obtained then require corrections due to well-characterized systematic deficiencies. The strengths are modified in three ways. The strengths are: (i) shifted down in E_γ (ranging from -0.5 MeV at low energies to -5 MeV at 21 MeV); (ii) folded with simple Lorentzians (E1 are given variable widths $\Gamma = 7 - A/45$ MeV, M1 are given fixed widths $\Gamma = 0.5$ MeV); and (iii) combined with correction terms added to account for strength to excited states:

$$\overleftarrow{f}_{\text{QRPA+0lim}}^{\text{E1}}(E_\gamma) = f_{\text{QRPA}}^{\text{E1}}(E_\gamma) + f_0 U / [1 + e^{(E_\gamma - \epsilon_0)}] \quad (14)$$

$$\overleftarrow{f}_{\text{QRPA+0lim}}^{\text{M1}}(E_\gamma) = f_{\text{QRPA}}^{\text{E1}}(E_\gamma) + C e^{-\eta E_\gamma}. \quad (15)$$

Here, U is the excitation energy of the decay nucleus in MeV, and f_0, ϵ_0, C , and η are free parameters adjusted to shell model calculations and experimental data for radiative decay [35]. The final modified calculations are denoted “D1M+DRPA+0lim”.

A. M1 strength in the pf -shell

We used two schemes to compute the M1 RSF in the pf -shell valence space using the GX1A interaction [74]. The full configuration interaction matrix dimension of ^{56}Fe in this space is more than 500 million (M-scheme). While converging a small number of levels is not difficult,

it would be impractical to compute and store the thousands of wave functions necessary to cover the full energy range up to about 20 MeV (after which the strength is negligible). We therefore apply the ILSF method and compare the results with another approach, namely, a basis-truncation scheme that reduces the computational cost of converging many levels.

As with ^{24}Mg , the shape of the ^{56}Fe M1 RSF evolves with excitation energy. As expected, the RSF built on the ground-state has no low-energy strength (Fig. 6a), while the RSF obtained when we average over many de-excited levels shows an exponential LEE (Fig. 6b). Unexpectedly, we find that the evolution proceeds with even higher energies. By quadrupling the number of excited levels included, we find that the slope of the LEE decreases (Fig. 6c). We can interpret this in light of the results of section III B, which showed that it is the energy of level d involved in the RSF, not the number of levels, that is responsible for the low-energy strength. The flattening trend is reinforced if we extend our calculations to even higher excitation energies (Fig. 6d), made possible by the ILSF method.

In the following, we discuss the four calculations in Fig. 6 (a-d) which include progressively higher energies and demonstrate the shape evolution of the M1 RSF.

(a) First, we used the LSF on the exactly converged ground state of our pf shell calculation. That is, we calculate $f_{d=1}^{\text{M1}}(E_\gamma)$. The overall shape converges after a few Lanczos iterations. However, to avoid introducing uncertainty from the Lorentzian folding procedure, we performed enough iterations (1000) such that the binned distribution has only a few empty bins at a bin size of $\Delta E = 500$ keV (see Fig. 6a). We find relatively good agreement with the zero-temperature D1M+QRPA [35]. We find essentially the same peak energy, without energy-shifting the strengths as was done for the QRPA calculation [35]. Interestingly, our calculation produces a long tail of strength above the peak. The strength around 3 MeV, which is thought to be attributable to a scissors mode [75], appears in similar locations in both calculations.

(b) To compute a RSF averaged over many ^{56}Fe levels d , we had to reduce the computational cost of converging the wave functions. We used the weak-entanglement approximation (WEA) [76, 77], an importance truncation scheme that has been shown to perform well for RSF calculations [78]. We give further details for the WEA calculations in Appendix D. Using 500 WEA wave functions, we compute the averaged radiative strength function $f_{(\text{SA})}^{\text{XL}}$ over all 500 levels (Fig. 6b). The highest energy level is around 9.9 MeV, which sets the upper-bound for photon energies. The resulting calculation is in agreement with the D1M+QRPA+0lim $T > 0$ shape [35, 73], which includes a phenomenological term inspired by LSSM calculations of M1 strengths (first proposed by Schwengner *et al.* [22]).

(c) By extending the previous calculation of the averaged RSF to use 2000 WEA wave functions, three

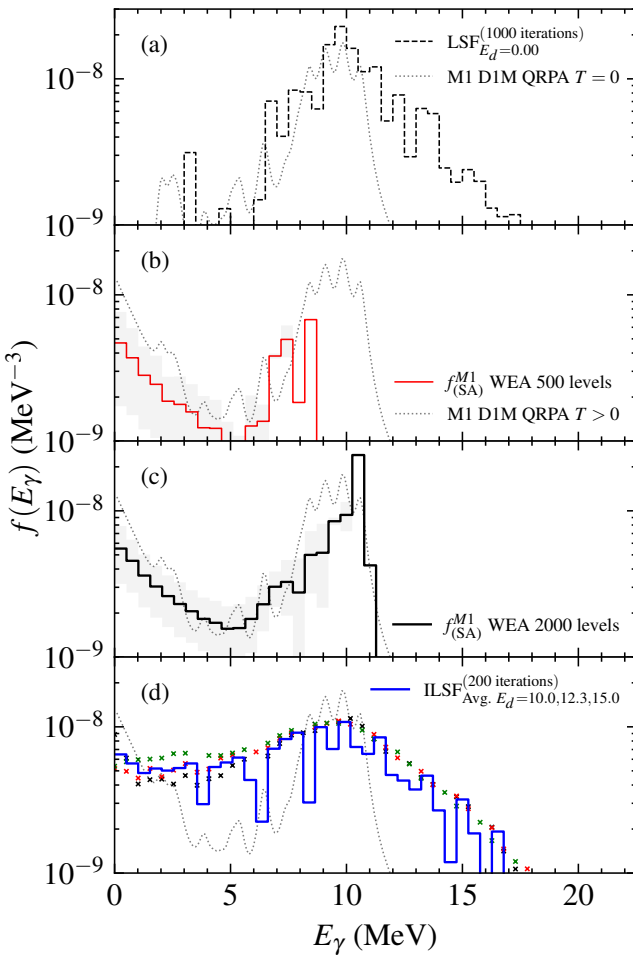


FIG. 6. The M1 RSF for ^{56}Fe for various energies of the de-excited level, computed within the pf shell with the GX1A [74] interaction. a) The LSSM LSF strength to the ground state is comparable to the D1M QRPA calculation at zero temperature. Our result produces more strength at higher energies. b) With the weak entanglement approximation (WEA), we reproduce the qualitative shape of D1M QRPA $T > 0$ calculation, which includes a phenomenological term fit to LSSM calculations. With only 500 levels, the calculation does not produce strength above 8.3 MeV. c) If we quadruple the number of WEA levels to 2000, we reach strength up to 10.7 MeV, including the dipole peak around 10 MeV. The distribution begins to flatten. d) We obtain the RSF up to 20 MeV by using the ILSF method introduced in the text, and averaging over partial RSFs for three levels above 10 MeV. Including higher excitations clearly leads to a flatter distribution of strength. Present calculations use $\Delta E = 500$ keV.

changes occur. The first is trivial: the RSF now reaches $E_\gamma = 10.7$ MeV (Fig. 6c). The second is that the standard deviation of the individual strengths decreases, as shown by the gray bands. This reduction can be interpreted in terms of Porter-Thomas fluctuations: as the nucleus reaches higher excitation energies, more transitions contribute to each E_γ bin, bringing the distribution

closer to the mean [13]. The third is that the LEE shape begins to flatten.

(d) The damping of the LEE slope (and increase in total strength) continues at higher excitation energies, as shown in Fig. 6d. Here, we converged three interior eigenstates (wave functions) at 10.0, 12.3, and 15.0 MeV using thick-restart block-Lanczos. Then, using the ILSF method previously discussed, we computed the average strength assuming the ELBA hypothesis. Using the ILSF method, we can predict the RSF above $E_\gamma = 20$ MeV. The highest photon energies involved with these transitions correspond to transitions from levels around $E_c = 30$ MeV; it would not be computationally possible to converge the number of individual levels to reach these energies with the brute-force method use above (even with the WEA). One might be concerned that states at these energies may not be well described in the pf -space alone. However, we repeated these calculations in the $sdpf$ valence space and found the results comparable.

The flattening of the M1 strength with excitation energy can be interpreted in view of earlier results. Karampagia *et al.* [30] showed the exponential LEE in shell model calculations is a feature of transitions constrained to a single orbit; as higher orbits are mixed into the model space, the strength is “quenched”, leading to a flatter distribution. Midtbø *et al.* [31] also showed that the M1 strength flattens as one moves away from a closed shell, which can be understood to follow from the same mixing of orbitals. For our results, mixing of valence space orbitals increases with excitation energy, rather than artificial model space restrictions or proximity to closed shells.

From the systematics of strength function sum rules [54], one should already anticipate that the total M1 strength of excited states should be larger than that of the ground state. What is novel about the present findings is an understanding of where (in photon energies) that extra strength appears, and the additional step of translating those strengths into reaction theory inputs.

We have shown that the M1 RSF strength distribution evolves slowly with the excitation energy of the levels involved. Despite this new subtlety, we arrive at the same conclusion from earlier LSSM calculations [26, 30, 31], which is that the M1 RSF cannot explain the LEE extracted from Oslo-type data. However, due to computational costs, no calculation of the E1-contributions to the LEE has yet been made for ^{56}Fe . We address this need in the next subsection.

B. E1 strength in the $sdpf$ -shell

To compute the E1 strengths, one must include, at a minimum, two or more single particle orbits in the model space with opposite parity and a difference in angular momentum of one unit. To meet this minimum we use the $sdpf$ shell model

space ($1d_{5/2}, 2s_{1/2}, 1d_{3/2}, 1f_{7/2}, 2p_{3/2}, 1f_{5/2}, 2p_{1/2}$) and the SDPFMU-DB interaction [79, 80]. It is likely that the $1g_{9/2}$ orbital plays a role in the GDR of ^{56}Fe , but there is not presently a robust interaction and model space publicly available to handle its inclusion. Inclusion of the $1g_{9/2}$ orbital may also influence the low-energy behavior of the RSF. This question should be investigated once a suitable interaction and model space become available.

The LSF on its own is insufficient to compute the RSF of ^{56}Fe in the $sdpf$ space, since the untruncated basis dimension (2×10^{15}) is too large to obtain even a single wave function. To reduce the basis to a manageable size, we used a truncation scheme based on energy centroids with the **tracer** code [81] and the **BIGSTICK** shell model code [61]. As in, Ref. [76], we assign to each orbital a an integer weight w_a . Each many-body configuration is given a total weight W which is the sum of the weights of the occupied orbitals. The M -scheme space is truncated by keeping all configurations with weights up to a maximum W_{\max} , defined relative to the minimum in the space W_{\min} : $W_{\text{ex}} = W_{\max} - W_{\min}$. We assigned the following weights w to each of the orbitals: $w(1d_{5/2}) = 1$; $w(2s_{1/2}) = 2$; $w(1d_{3/2}) = 0$; $w(1f_{7/2}) = 3$; $w(2p_{3/2}) = 4$; $w(1f_{5/2}) = 5$; $w(2p_{1/2}) = 6$. This choice of weights approximates a truncation based upon the centroids (average energies) of orbital configurations [82, 83]. With $W_{\text{ex}} = 11$, ^{56}Fe has an M -scheme dimension of 520 million.

With the above approximations, we find the following results. The E1 RSF built on the ground state with the LSF method has no strength below about $E_{\gamma} = 6$ MeV, which is where the first 1^- level occurs (Fig 7a). This is the qualitative result one would expect to observe from E1 photo-absorption on the ground state of ^{56}Fe .

To calculate the RSF to the ground state, we first used standard Lanczos to converge the ^{56}Fe ground state wave function. We performed no folding with Lorentzians or systematic shifting of strength. The strength averaging was performed with a bin width of $\Delta E = 500$ keV. To compute the E1 transitions, we used standard one-body operators with effective charges $e_p = +N/A = 30/56 = 0.536$ and $e_n = -Z/A = -26/56 = -0.464$. The harmonic oscillator basis length $b = \sqrt{\hbar}/(m\omega)$ was set to the Blomqvist and Molinari prescription [84]: $b^2 = 41.467/(45A^{-1/3} - 25A^{-2/3})$ fm 2 , which for ^{56}Fe gives $b = 2.03$ fm. To remove spurious center of mass motion, we included a Lawson term [85] in all of our $sdpf$ calculations, both while converging the pivot wave functions and when applying the LSF method. We verified our resulting wave functions have COM energies less than 0.001 MeV, which is negligible compared to their roughly 500 MeV relative binding energies.

Next, when we include higher excitation energies in the RSF calculation, strength appears below the photo-absorption threshold (≈ 6 MeV) which was not seen in the RSF to the ground state (Fig. 7b). Calculation of this E1 LEE was only made possible with the ILSF method if we first applied the same basis-truncation used to obtain

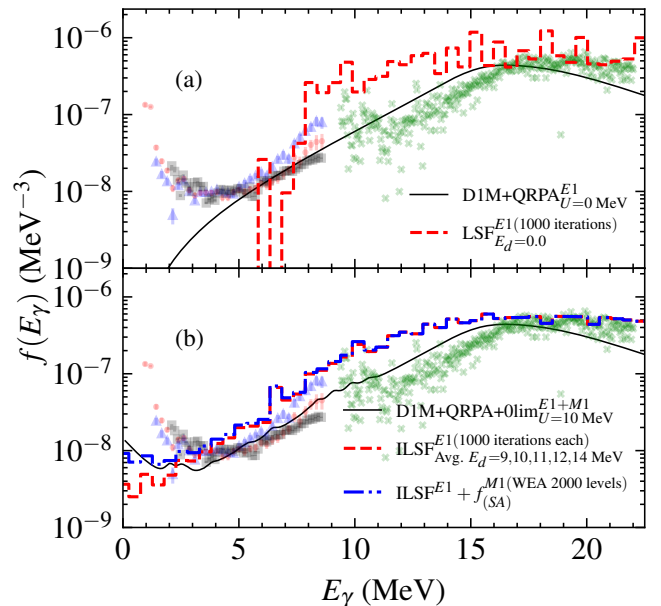


FIG. 7. The LEE observed in several experiments cannot be explained by a combination of radiative M1 and E1 strength with the present $sdpf$ -valence-space calculations. We show (a) shell model calculations of the E1 RSF involving only the ground state of ^{56}Fe using our LSF method, and (b) the excited-state E1 RSF generated with our ILSF method using five levels from 9 MeV to 14 MeV. The data shown are from ^3He scattering by Voinov *et al.* [69] (red dots) and Algin *et al.* [70] (blue triangles), $(p, p'\gamma)$ scattering by Larsen *et al.* [71] (black squares), and proton-inelastic, isovector giant dipole resonance data from Jingo *et al.* [72] (green crosses).

the $sdpf$ ground state.

To apply the ILSF method, we partially converged five $j_d = 0$ levels near the neutron separation energy $S_n(^{56}\text{Fe}) = 11.197$ MeV. As in the pf -space calculations, our wave functions were obtained with thick-restart Lanczos, with the additional cJ^2 term to push-out $J > 0$ levels. We performed a total of 800 iterations, which yielded five levels within $0.004\hbar$ of $J = 0\hbar$, and excitation energies $E = 9.05, 10.2, 11.3, 12.5, 13.7$ MeV. After applying the same E1 operator as for the ground state RSF, we applied 1000 Lanczos iterations to each interior pivot.

Summing together the E1 strength from ILSF and the M1 strength from the WEA calculation with 2000 levels, we present the total RSF for ^{56}Fe computed in the $sdpf$ model space. We chose to use this particular set of M1 strengths because it aligns with the excitation energies accessed in the Oslo measurements (up to around the neutron separation energy). However, the incompatibility with the Oslo data persists in all of our M1 calculations. The E1 strength dominates the low-energy RSF above 3 MeV, below which the M1 strength dominates. Within the present $sdpf$ model space and interaction, the shell model calculation cannot reproduce the RSF extracted from Oslo data below 3 MeV. The remaining

discrepancy below 3 MeV is between a factor of 3 to 10.

We find a GDR energy centroid similar to that of the D1M+QRPA result (~ 16 MeV). Both of these microscopic predictions are low relative to the experimental value around 18.6 MeV, and low relative to the systematic estimate which predicts a double peak at 17.08 and 20.12 MeV [66]. Much of the shell model strength is shifted lower in energy, seen as surplus strength between 8 and 15 MeV. An isospin decomposition reveals this energy shift is split by isospin-conserving transitions ($\Delta T = 0$) which peak at 15 MeV, and the isospin-changing transitions ($\Delta T = 1$) peak near 22 MeV.

V. CONCLUSION

We have shown that a level-density-free definition of the radiative strength function formula can simplify calculations, clarify interpretation in terms of sum rules, and enable the LSF method to be applied. The LSF method essentially resolves the moments of the radiative strength distribution, rather than generating all individual transition probabilities, which is the current practice. We showed one can approximate the full RSF with just a few Lanczos pivots, owing to the ELBA hypothesis.

The present results reveal that the M1 strength of ^{56}Fe evolves smoothly as a function of excitation energy. Strength to the ground state only (corresponding to a photo-absorption measurement) has the expected single-GDR shape. An average over strength to many excited states up to 10 MeV reveals the expected exponential LEE. However, as we move to higher energies, the RSF shape flattens to a nearly constant distribution below the M1 GDR. Smooth evolution of total strength with excitation energy is expected from the ELBA hypothesis [54, 56]. The shape-evolution of the strength *distribution* follows as a logical extension of the ELBA hypothesis, and can be understood in analogy to the known correlation with nearness to a closed shell [31] or artificial model space restrictions [30].

Using our novel ILSF approach, we also presented the first LSSM description of the radiative strength function of ^{56}Fe , including M1 and E1 contributions from $E_\gamma = 0$ to 20 MeV. The results suggest that the $sdpf$ valence space, lacking the $g_{9/2}$ orbital, is insufficient to accurately describe the E1 GDR response of ^{56}Fe , though future calculations will help in clarifying the situation. The discrepancy relative to the Oslo-type measurements below 3 MeV also remains unresolved. We leave development of a robust model space and effective interaction including the $g_{9/2}$ orbital to future work. For the purposes of constraining neutron capture rates, it will also be important to include uncertainty quantification based on the underlying effective interaction similar to [86].

RSFs were originally developed assuming the strong Brink-Axel hypothesis so that radiative decay could be constrained by photo-absorption experiments. As microscopic models become favored for their predictive power,

this restriction no longer serves its use. Our results and the ILSF method presented here instead further support the energy-localized Brink-Axel hypothesis, indicating that RSFs should evolve with the energy of the de-excited level. Looking forward, we suggest that current HF codes could be improved by accepting tabulated RSFs which depend on both E_γ and E_d , the energy of the de-excited level.

ACKNOWLEDGMENTS

This work was performed under the auspices of the U.S. Department of Energy by Lawrence Livermore National Laboratory under Contract DE-AC52-07NA27344, with support from Laboratory Directed Research and Development project No. 24-ERD-023. This material is also based upon work by CWJ supported by the U.S. Department of Energy, Office of Science, Office of Nuclear Physics, under Award Number DE-FG02-03ER41272, and work done by OCG supported by the LLNL WPD ACT award program. We thank the broader RETRO collaboration for providing useful feedback.

Appendix A: LDF-RSF in relation to other quantities

We show how our RSF, Eq. (10), relates to: sum-rule strength functions, the sum-rule expression for photo-absorption, and generalized transmission coefficients.

1. Relation to sum-rule strength functions

Following the discussion in Section II, one can further show that the energy-differential, time-reversed version of the RSF, Eq. (10) has the same form as the sum-rule strength function, Eq. (6). That is, if we suppose that the RSF is an energy-average of some differential strength df_d^{XL}/dE_c , then we can write:

$$f_d^{XL}(E_\gamma) = \frac{1}{\Delta E} \int_{E_c - \Delta E/2}^{E_c + \Delta E/2} \frac{df_d^{XL}}{dE_c}(E_\gamma) dE_c, \quad (\text{A1})$$

where we are not selecting a particular spin j_c as in Eq. (10). It follows that the differential strength function must be:

$$\frac{df_d^{XL}}{dE_c}(E_\gamma) = \sum_c \delta(E_c - E_d + E_\gamma) \frac{\Gamma_{d \leftarrow c}^{XL}}{E_\gamma^{2L+1}}. \quad (\text{A2})$$

Eq. (A2) and Eq. (6) have similar forms in terms of B -values. The key differences are: (i) the RSF contains additional constants from in the definition of Γ_{dc}^{XL} , (ii) the RSF is often given for specific spins j_c , and (iii) the RSF always sums over the index c with $E_c > E_d$, whereas the sum-rule SF sums over all $f \neq i$; when S^{XL} is built

on the ground state, it is proportional to the absorption cross-section, but df_d^{XL}/dE_c contains the time-reversed statistical factors and must be combined with the factors in Eq. (7). Finally, because the RSF does not sum over all levels in the model space (only those with $E_c > E_d$), the RSF does not strictly obey sum rules.

2. Relation to other expressions for capture

As noted in Blatt and Weisskopf [1] (p. 392), HF theory is constructed such that the absorption cross section is proportional to the probability for the decay of the compound nucleus, hence the B -values for $c \rightarrow d$ in the definition of the RSF, Eq. (10). However, the shell-model expression for photo-absorption is typically written as [52, 53, 65]:

$$\sigma_\gamma^{XL}(E_\gamma) = \frac{8\pi^3(L+1)k_\gamma^{2L-1}}{L[(2L+1)!!]^2} S^{XL}(E_d, E_\gamma), \quad (\text{A3})$$

where $S^{XL}(E_d, E_\gamma)$ is given by Eq. (6) (with B -values for $d \rightarrow c$, summed over c). Clearly, the RSF (10) is not time-reversible ($\overleftarrow{f} \neq \overrightarrow{f}$) since $B_{c \leftarrow d}^{XL} \neq B_{d \leftarrow c}^{XL}$. So, how do we reconcile these two expressions for photo-absorption?

As a consistency check, we fully expand the photo-absorption cross section Eq. (7) to show it is equivalent to Eq. (A3). We substitute the transmission coefficients, Eq.(9), into the HF cross section Eq. (7) and combine the sums over j_c and c :

$$\langle \sigma_\gamma^{XL} \rangle(E_\gamma) = \frac{\pi^2}{k_\gamma^2} \sum_{j_c} \frac{(2j_c+1)}{(2j_d+1)} \frac{1}{\Delta E} \sum_{c'} \delta_{j_{c'} j_c} \Gamma_{d \leftarrow c'}^{XL}(E_\gamma) \quad (\text{A4})$$

$$= \frac{\pi^2}{k_\gamma^2} \frac{1}{\Delta E} \sum_c \frac{(2j_c+1)}{(2j_d+1)} \Gamma_{d \leftarrow c}^{XL}(E_\gamma). \quad (\text{A5})$$

Next, we expand the widths in terms of squared matrix elements. After cancellation of statistical factors we have:

$$\begin{aligned} \langle \sigma_\gamma^{XL} \rangle(E_\gamma) &= \frac{8\pi^3(L+1)k_\gamma^{2L-1}}{L[(2L+1)!!]^2} \frac{1}{\Delta E} \sum_c \frac{1}{2j_d+1} \\ &\times \sum_{m_c m_d M} |\langle j_d m_d | \mathcal{M}^{XLM} | j_c m_c \rangle|^2 \quad (\text{A6}) \end{aligned}$$

Using the definition of B -values and the symmetry $|\langle j_d m_d | \mathcal{M}^{XLM} | j_c m_c \rangle|^2 = |\langle j_c m_c | \mathcal{M}^{XLM} | j_d m_d \rangle|^2$, we obtain a cross section containing the B -values for $d \rightarrow c$:

$$\langle \sigma_\gamma^{XL} \rangle(E_\gamma) = \frac{8\pi^3(L+1)k_\gamma^{2L-1}}{L[(2L+1)!!]^2} \frac{1}{\Delta E} \sum_c B_{c \leftarrow d}^{XL}, \quad (\text{A7})$$

which is the energy-average of Eq. (A3).

3. Relation to generalized transmission coefficients

In the case of photo-absorption, the RSF Eq. (10) should be computed for a single level $|j_d\rangle$, the level absorbing photons. But what about for radiative decay? In the case of decay from a bin (E_c, j_c, π_c) to another de-excited bin (E_d, j_d, π_d) , a HF code computes the *generalized transmission coefficient* as:

$$\mathcal{T}^{XL}(E_\gamma, E_c) = \int_{E_d - \Delta E/2}^{E_d + \Delta E/2} T_d^{XL}(E_\gamma) \rho(E_d) dE_d, \quad (\text{A8})$$

where the spin and parity selection rules must be obeyed, but are not explicitly shown. No additional statistical factor is necessary, since, by construction, the reduced transition probabilities $B_{d \leftarrow c}^{XL}$ contained in Eq. (10) contain the correct factors already: a sum over de-excited magnetic substates m_d and an average over CN magnetic substates m_c .

Appendix B: LSF implementation

We use the BIGSTICK shell model code to apply the Lanczos strength-function (LSF) method [61]. For a more detailed description of the LSF method, we recommend the appendix of Herrera *et al.* [56]. Here, we give a cursory introduction while highlighting key details relevant for computing radiative strength functions.

The LSF method uses a modified Lanczos algorithm to compute the matrix elements needed to compute radiative strength functions, given by sums over $|\langle \psi_c | \mathcal{M}^{XL} | \psi_d \rangle|^2$ for an electromagnetic operator \mathcal{M}^{XL} . The trick is to first create a Lanczos pivot vector by applying the transition operator to the initial wave function: $|\psi_0\rangle = \mathcal{M}^{XL}|\psi_d\rangle$. Then, the Lanczos algorithm is applied, generating approximate eigenstates $|\tilde{\psi}\rangle$ of the Hamiltonian. For each $|\tilde{\psi}\rangle$, one computes the squared overlap with the pivot: $|\langle \tilde{\psi} | \psi_0 \rangle|^2$, which are the required matrix elements. Because we energy-average over c to obtain the RSF, the fact that the Lanczos eigenstates $|\tilde{\psi}_c\rangle$ are only approximately converged (and thus a superposition of nearby levels) becomes unimportant [56, 67].

The radiative strength function to a particular de-excited state d has the form:

$$f_d^{XL}(E_\gamma) = C^{XL} \frac{1}{\Delta E} \sum_c B_{dc}^{XL}, \quad (\text{B1})$$

(we omit spin selection for brevity) where,

$$C^{XL} = \frac{8\pi(L+1)}{L[(2L+1)!!]^2} \left(\frac{1}{\hbar c} \right)^{2L+1}. \quad (\text{B2})$$

Because the B -values, Eq. (4), are defined with a sum over all “final” magnetic states and an average over “initial” magnetic states, the order $d < c$ is important. The

B -values are computed within a single- M basis using the Wigner-Eckart theorem:

$$B_{dc}^{XL} = \frac{1}{2j_c + 1} |\langle j_d | \mathcal{M}^{XL} | j_c \rangle|^2 \quad (\text{B3})$$

$$= \frac{2j_d + 1}{2j_c + 1} \left| \frac{\langle j_d m | \mathcal{M}^{XL0} | j_c m \rangle}{(j_c m L 0 | j_d m)} \right|^2. \quad (\text{B4})$$

By choosing the Lanczos pivot to be an excited state, $\mathcal{M}^{XL}|j_d m_d\rangle$, the LSF algorithm yields the unreduced amplitudes: $|\langle \tilde{\psi}_c | \mathcal{M}^{XL} | j_d m_d \rangle|^2$. However, in an $M = 0$ basis, certain vector coupling coefficients are zero due to symmetries ($\langle j_i 0 j_f 0 | L 0 \rangle = 0$ when $j_i + j_f - L$ is odd), which results in “missing” $L = 1$ strengths when $j_i = j_f$ and j_i, j_f are integers, which must be recovered (although, we find their effect is negligible).

For an arbitrary choice of the pivot vector spin j_d , the states $\tilde{\psi}_c$ produced by the Lanczos iterations will have a superposition of multiple j_c , since \mathcal{M}^{XL} is not a scalar operator. This makes it difficult to compute the vector coupling constants in Eq. (B4); one must then first project out states of good J . However, if we choose a $j_d = 0$ wave function, only $j_c = 1$ pivots are produced. Using the relation $\langle j_1 0 j_2 0 | 00 \rangle^2 = \delta_{j_1, j_2} / (2j_1 + 1)$, one can further show that for $j_d = 0$:

$$B_{dc}^{XL}(j_d = 0) = |\langle j_d m | \mathcal{M}^{XL} | j_c m \rangle|^2 \quad (\text{B5})$$

$$= |\langle j_c m | \mathcal{M}^{XL} | j_d m \rangle|^2. \quad (\text{B6})$$

Therefore, using any $j_d = 0$ wave function to create the pivot greatly simplifies the calculation. This restriction should be acceptable since: (i) HF theory already assumes spin-independent RSFs, (ii) past shell model studies have found minimal dependence on spin and parity [26, 30], and (iii) our WEA calculations support the same conclusion (Fig. 8). Finally, the LSF RSF is computed in an $M = 0$ basis as:

$$f_{d(j_d=0)}^{XL}(E_\gamma) = C^{XL} \frac{1}{\Delta E} \sum_c |\langle j_c 0 | \mathcal{M}^{XL} | j_d 0 \rangle|^2. \quad (\text{B7})$$

The spin-selected version is recovered by inserting δ_{j_c, j'_c} .

Appendix C: Constants and units

For convenience, we provide numerical values for the constant, Eq. (B2), in order to produce RSFs with units of $\text{MeV}^{-(2L+1)}$ when the units of the B -values are absorbed into the constant. For EL transitions, the B -values had units of $e^2(\text{fm})^{2L}$, where fm is taken to be unity. With $e^2 = \alpha \hbar c$ (with CGS units, $1 = 4\pi\epsilon_0$) where $\hbar c = 197.327 \text{ MeV fm}$ and the dimensionless fine-

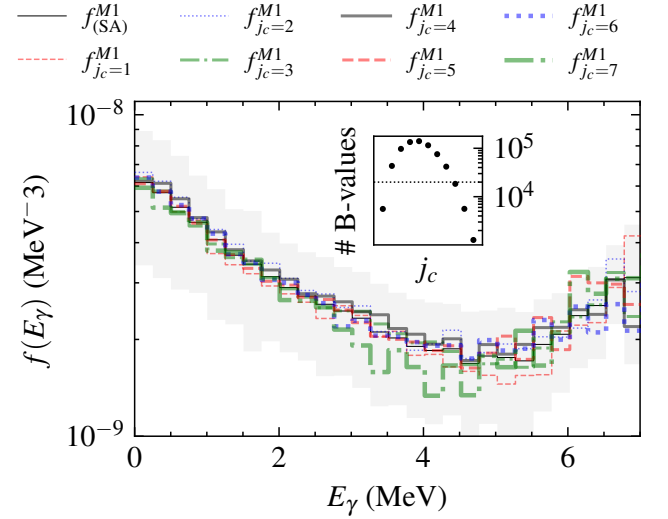


FIG. 8. The RSF f_{j_c} is independent of the spin of the decaying levels j_c , as illustrated by plotting the RSF from Fig. 6(c) for different j_c . Deviations of specific f_{j_c} arise when too few B -values contribute, which occurs when there are a limited number of levels with that spin included in the calculation. The inset shows the number of B -values used in each f_{j_c} for $j_c = 0, 1, \dots, 10\hbar$. RSFs computed from few B -values are susceptible to Porter-Thomas fluctuations (see section III A), so we only plot f_{j_c} with more than $2 \cdot 10^4$ contributing B -values, excluding $j_c = 0, 8, 9, 10\hbar$.

structure constant $\alpha = 1/137.036$:

$$C^{E1} = \frac{16\pi}{9} \left(\frac{1}{\hbar c} \right)^3 e^2(\text{fm})^2 = 1.04669 \cdot 10^{-6} \text{ MeV}^{-2}, \quad (\text{C1})$$

$$C^{E2} = \frac{24\pi}{30} \left(\frac{1}{\hbar c} \right)^5 e^2(\text{fm})^4 = 5.83384 \cdot 10^{-12} \text{ MeV}^{-4}. \quad (\text{C2})$$

For ML transitions, the B -values had units of $\mu_N^2(\text{fm})^{2L-2}$; μ_N is nuclear magneton which in CGS units is $\mu_N = 0.105154e$ fm. With these constants,

$$C^{M1} = \frac{16\pi}{9} \left(\frac{1}{\hbar c} \right)^3 \mu_N^2 = 1.15737 \cdot 10^{-8} \text{ MeV}^{-2}. \quad (\text{C3})$$

Appendix D: Weak entanglement approximation

An alternative method to reduce the computational cost of computing shell model radiative strength functions is to use an appropriate many-body truncation to reduce the model space. For this purpose, we use the weak entanglement approximation (WEA) [76, 77] to solve for the lowest 500 wave functions, and then the lowest 2000 wave functions. The WEA is an importance truncation method that selects proton and neutron basis

components in the limit of zero proton-neutron entanglement. It has been shown that the method performs well for M1 RSF calculations [78]. We use a WEA basis constructed with 10-percent of the proton and neutron subspaces, which yields model dimensions reduced by a factor of 1000. (The largest J-scheme dimension we diagonalize, for $J = 5$, is $5.3 \cdot 10^5$). Using this scheme, our

WEA ground state energy is within 100 keV (.05%) of the untruncated value, which is comparable to typical uncertainties originating from the effective interaction [60, 86]. We separately converged the lowest 500 levels for each J from $J = 0$ to $J = 10$ and retain 500 or 2000 levels with the lowest energies.

[1] J. Blatt and V. Weisskopf, *Theoretical Nuclear Physics*, Dover Books on Physics Series (Dover Publications, 1991).

[2] A. Koning, S. Hilaire, and S. Goriely, The European Physical Journal A **59**, 10.1140/epja/s10050-023-01034-3 (2023).

[3] W.E. Ormand, *Monte Carlo Hauser-Feshbach Computer Code System to Model Nuclear Reactions: YAHFC*, Tech. Rep. (Lawrence Livermore National Lab.(LLNL), Livermore, CA (United States), 2021).

[4] T. Kawano, Coh3: The coupled-channels and hauser-feshbach code, in *Springer Proceedings in Physics* (Springer International Publishing, 2020) p. 27–34.

[5] M. Herman, R. Capote, B. V. Carlson, P. Oblozinsky, M. Sin, A. Trkov, H. Wienke, and V. Zerkin, Nuclear Data Sheets **108**, 2655 (2007).

[6] P. G. Young, E. D. Arthur, and M. B. Chadwick, *Comprehensive nuclear model calculations: Introduction to the theory and use of the GNASH code*, Tech. Rep. (Los Alamos National Lab., NM (United States), 1992).

[7] M. Mumpower, R. Surman, G. McLaughlin, and A. Aprahamian, Progress in Particle and Nuclear Physics **86**, 86 (2016).

[8] M. R. Mumpower, T. Kawano, J. L. Ullmann, M. Krtička, and T. M. Sprouse, Physical Review C **96**, 10.1103/physrevc.96.024612 (2017).

[9] M. Arnould and S. Goriely, Progress in Particle and Nuclear Physics **112**, 103766 (2020).

[10] A. C. Hayes, Reports on Progress in Physics **80**, 026301 (2017).

[11] K. Kolos, V. Sobes, R. Vogt, C. E. Romano, M. S. Smith, L. A. Bernstein, D. A. Brown, M. T. Burkey, Y. Danon, M. A. Elsawi, B. L. Goldblum, L. H. Heilbronn, S. L. Hogle, J. Hutchinson, B. Loer, E. A. McCutchan, M. R. Mumpower, E. M. O’Brien, C. Percher, P. N. Peplowski, J. J. Ressler, N. Schunck, N. W. Thompson, A. S. Voyles, W. Wieselquist, and M. Zerkle, Phys. Rev. Res. **4**, 021001 (2022).

[12] D. Brink, *Some aspects of the interaction of light with matter*, Ph.D. thesis, University of Oxford (1955).

[13] P. Axel, Physical Review **126**, 671–683 (1962).

[14] J. Kopecky and M. Uhl, Physical Review C **41**, 1941–1955 (1990).

[15] J. Kopecky, M. Uhl, and R. E. Chrien, Phys. Rev. C **47**, 312 (1993).

[16] S. Goriely and V. Plujko, Phys. Rev. C **99**, 014303 (2019).

[17] J. E. Escher, J. T. Harke, F. S. Dietrich, N. D. Sciullo, I. J. Thompson, and W. Younes, Reviews of Modern Physics **84**, 353 (2012).

[18] A. C. Larsen, M. Guttormsen, M. Krtička, E. Šešták, A. Bürger, A. Görgen, H. T. Nyhus, J. Rekstad, A. Schiller, S. Siem, H. K. Toft, G. M. Tveten, A. V. Voinov, and K. Wikan, Physical Review C: Nuclear Physics **83**, 034315 (2011).

[19] A. C. Larsen, J. E. Midtbø, M. Guttormsen, T. Renstrøm, S. N. Liddick, A. Spyrou, S. Karampagia, B. A. Brown, O. Achakovskiy, S. Kamerdzhiev, D. L. Bleuel, A. Couture, L. C. Campo, B. P. Crider, A. C. Dombos, R. Lewis, S. Mosby, F. Naqvi, G. Perdikakis, C. J. Prokop, S. J. Quinn, and S. Siem, Physical Review C: Nuclear Physics **97**, 054329 (2018).

[20] V. W. Ingeberg, S. Siem, M. Wiedeking, A. Choplin, S. Goriely, L. Siess, K. J. Abrahams, K. Arnswald, F. Bello Garrote, D. L. Bleuel, J. Cederkäll, T. L. Christoffersen, D. M. Cox, H. De Witte, L. P. Gaffney, A. Görgen, C. Henrich, A. Illana, P. Jones, B. V. Kheswa, T. Kröll, S. N. T. Majola, K. L. Malatji, J. Ojala, J. Pakarinen, G. Rainovski, P. Reiter, M. von Schmid, M. Seidlitz, G. M. Tveten, N. Warr, and F. Zeiser (The ISOLDE Collaboration), Phys. Rev. C **111**, 015803 (2025).

[21] B. L. Berman and S. C. Fultz, Reviews of Modern Physics **47**, 713 (1975).

[22] R. Schwengner, S. Frauendorf, and A. C. Larsen, Physical Review Letters **111**, 232504 (2013).

[23] S. Frauendorf, M. Beard, M. Mumpower, R. Schwengner, and K. Wimmer, EPJ Web of Conferences **93**, 04002 (2015).

[24] S. G. Kadmenkii, V. P. Markushev, and V. I. Furman, Soviet Journal of Nuclear Physics **37**, 165 (1983), original in Russian: Yad. Fiz. 37, 277 (1983).

[25] R. Schwengner, R. Massarczyk, B. A. Brown, R. Beyer, F. Dönnau, M. Erhard, E. Grosse, A. R. Junghans, K. Kosev, C. Nair, G. Rusev, K. D. Schilling, and A. Wagner, Physical Review C: Nuclear Physics **81**, 054315 (2010).

[26] B. A. Brown and A. C. Larsen, Physical Review Letters **113**, 252502 (2014).

[27] M. Martini, S. Péru, S. Hilaire, S. Goriely, and F. Lechaftois, Phys. Rev. C **94**, 014304 (2016).

[28] K. Sieja, Phys. Rev. Lett. **119**, 052502 (2017).

[29] R. Schwengner, S. Frauendorf, and B. A. Brown, Phys. Rev. Lett. **118**, 092502 (2017).

[30] S. Karampagia, B. A. Brown, and V. Zelevinsky, Phys. Rev. C **95**, 024322 (2017).

[31] J. E. Midtbø, A. C. Larsen, T. Renstrøm, F. L. Bello Garrote, and E. Lima, Physical Review C: Nuclear Physics **98**, 064321 (2018).

[32] S. Frauendorf and R. Schwengner, Physical Review C: Nuclear Physics **105**, 034335 (2022).

[33] P. Fanto and Y. Alhassid, Phys. Rev. C **109**, L031302 (2024).

[34] F.-Q. Chen, Y. F. Niu, Y. Sun, and M. Wiedeking, Phys. Rev. Lett. **134**, 082502 (2025).

[35] S. Goriely, S. Hilaire, S. Péru, and K. Sieja, Physical Review C: Nuclear Physics **98**, 014327 (2018).

[36] T. Li, N. Schunck, and M. Grosskopf, Phys. Rev. C **110**, 034317 (2024).

[37] S. Péru, S. Goriely, and S. Hilaire, EPJ Web of Conferences **322**, 06003 (2025).

[38] S. Goriely, S. Péru, and S. Hilaire, Physics Letters B **868**, 139677 (2025).

[39] Y. Xu, S. Goriely, M. Krčíčka, and E. Khan, Phys. Rev. C **113**, 014306 (2026).

[40] K. Sieja, The European Physical Journal A **59**, 10.1140/epja/s10050-023-01067-8 (2023).

[41] S. N. Liddick, A. C. Larsen, M. Guttormsen, A. Spyrou, B. P. Crider, F. Naqvi, J. E. Midtbø, F. L. Bello Garrote, D. L. Bleuel, L. Crespo Campo, A. Couture, A. C. Dombos, F. Giacoppo, A. Görgen, K. Hadynska-Klek, T. W. Hagen, V. W. Ingeberg, B. V. Kheswa, R. Lewis, S. Mosby, G. Perdikakis, C. J. Prokop, S. J. Quinn, T. Renstrøm, S. J. Rose, E. Sahin, S. Siem, G. M. Tveten, M. Wiedeking, and F. Zeiser, Physical Review C **100**, 10.1103/physrevc.100.024624 (2019).

[42] J. K. Dahl, A.-C. Larsen, N. Shimizu, and Y. Utsuno, Microscopic study of the low-energy enhancement in the gamma-decay strength of ^{50}V (2025), arXiv:2510.23779 [nucl-th].

[43] F. Naqvi, A. Simon, M. Guttormsen, R. Schwengner, S. Frauendorf, C. S. Reingold, J. T. Harke, N. Cooper, R. O. Hughes, S. Ota, and A. Saastamoinen, Physical Review C: Nuclear Physics **99**, 054331 (2019).

[44] J. Rekstad, A. Henriquez, F. Ingebretsen, G. Midttun, B. Skaali, R. Øyan, J. Wikne, T. Engeland, T. F. Thorsteinsen, E. Hammaren, and E. Liukkonen, Physica Scripta **T5**, 45–50 (1983).

[45] A. Schiller, L. Bergholt, M. Guttormsen, E. Melby, J. Rekstad, and S. Siem, Nuclear Instruments and Methods in Physics Research Section A: Accelerators, Spectrometers, Detectors and Associated Equipment **447**, 498 (2000).

[46] W. Hauser and H. Feshbach, Physical Review **87**, 366 (1952).

[47] G. A. Bartholomew, E. D. Earle, A. J. Ferguson, J. W. Knowles, and M. A. Lone, in *Advances in Nuclear Physics: Volume 7*, edited by M. Baranger and E. Vogt (Springer US, Boston, MA, 1973) pp. 229–324.

[48] J. Kopecký and I. Tomandl, Phys. Rev. C **111**, 044606 (2025).

[49] A. Edmonds, *Angular Momentum in Quantum Mechanics*, Investigations in Physics Series (Princeton University Press, 1957).

[50] P. Brussard and P. Glaudemans, *Shell-Model Applications in Nuclear Spectroscopy* (North-Holland Publishing Company, Amsterdam, 1977).

[51] J. Suhonen, *From Nucleons to Nucleus: Concepts of Microscopic Nuclear Theory*, Theoretical and Mathematical Physics (Springer, Berlin, Germany, 2007).

[52] P. Ring and P. Schuck, *The Nuclear Many-Body Problem* (Springer Science & Business Media, New York, 2004).

[53] Y. Utsuno, N. Shimizu, T. Otsuka, S. Ebata, and M. Honma, Progress in Nuclear Energy **82**, 102 (2015).

[54] C. W. Johnson, Physics Letters B **750**, 72 (2015).

[55] I. J. Thompson and F. M. Nunes, *Nuclear Reactions for Astrophysics: Principles, Calculation and Applications of Low-Energy Reactions* (Cambridge University Press, 2009).

[56] R. A. Herrera, C. W. Johnson, and G. M. Fuller, Physical Review C: Nuclear Physics **105**, 015801 (2022).

[57] E. Caurier, G. Martinez-Pinedo, F. Nowacki, A. Poves, and A. P. Zuker, Reviews of Modern Physics **77**, 427 (2005).

[58] R. Whitehead, A. Watt, and D. Kelvin, Physics Letters B **89**, 313–315 (1980).

[59] S. Bloom, Progress in Particle and Nuclear Physics **11**, 505–528 (1984).

[60] B. A. Brown and W. A. Richter, Physical Review C: Nuclear Physics **74**, 034315 (2006).

[61] C. W. Johnson, W. E. Ormand, K. S. McElvain, and H. Shan, BIGSTICK: A flexible configuration-interaction shell-model code (2018).

[62] C. E. Porter and R. G. Thomas, Phys. Rev. **104**, 483 (1956).

[63] L. C. Campo, M. Guttormsen, F. L. B. Garrote, T. K. Eriksen, F. Giacoppo, A. Görgen, K. Hadynska-Klek, M. Klintefjord, A. C. Larsen, T. Renstrøm, E. Sahin, S. Siem, A. Springer, T. G. Tornyi, and G. M. Tveten, Phys. Rev. C **98**, 054303 (2018).

[64] M. Markova, A. C. Larsen, P. von Neumann-Cosel, S. Bassauer, A. Görgen, M. Guttormsen, F. L. B. Garrote, H. C. Berg, M. M. Bjørøen, T. K. Eriksen, D. Gjestvang, J. Isaak, M. Mbabane, W. Paulsen, L. G. Pedersen, N. I. J. Pettersen, A. Richter, E. Sahin, P. Scholz, S. Siem, G. M. Tveten, V. M. Valsdottir, and M. Wiedeking, Phys. Rev. C **106**, 034322 (2022).

[65] M. K. G. Kruse, W. E. Ormand, and C. W. Johnson, The European Physical Journal A **55**, 10.1140/epja/i2019-12905-1 (2019).

[66] R. Capote, M. Herman, P. Obložinský, P. Young, S. Goriely, T. Belgya, A. Ignatyuk, A. Koning, S. Hilaire, V. Plujko, M. Avrigeanu, O. Bersillon, M. Chadwick, T. Fukahori, Z. Ge, Y. Han, S. Kailas, J. Kopecký, V. Maslov, G. Reffo, M. Sin, E. Sh. Soukhovitskii, and P. Talou, Nuclear Data Sheets **110**, 3107 (2009).

[67] C. W. Johnson, K. A. Luu, and Y. Lu, Journal of Physics G: Nuclear and Particle Physics **47**, 105107 (2020).

[68] K. Wu and H. D. Simon, SIAM Journal on Matrix Analysis and Applications **22**, 602 (2000).

[69] A. Voinov, E. Algin, U. Agvaanluvsan, T. Belgya, R. Chankova, M. Guttormsen, G. E. Mitchell, J. Rekstad, A. Schiller, and S. Siem, Phys. Rev. Lett. **93**, 142504 (2004).

[70] E. Algin, U. Agvaanluvsan, M. Guttormsen, A. C. Larsen, G. E. Mitchell, J. Rekstad, A. Schiller, S. Siem, and A. Voinov, Phys. Rev. C **78**, 054321 (2008).

[71] A. C. Larsen, N. Blasi, A. Bracco, F. Camera, T. K. Eriksen, A. Görgen, M. Guttormsen, T. W. Hagen, S. Leoni, B. Million, H. T. Nyhus, T. Renstrøm, S. J. Rose, I. E. Ruud, S. Siem, T. Tornyi, G. M. Tveten, A. V. Voinov, and M. Wiedeking, Phys. Rev. Lett. **111**, 242504 (2013).

[72] M. Jingo, E. Z. Buthelezi, J. Carter, G. R. J. Cooper, R. W. Fearick, S. V. Förtsch, C. O. Kureba, A. M. Krumbholz, P. von Neumann-Cosel, R. Neveling, P. Papka, I. Poltoratska, V. Y. Ponomarev, A. Richter, E. Sideras-Haddad, F. D. Smit, J. A. Swartz, A. Tamii, and I. T. Usman, The European Physical Journal A **54**, 10.1140/epja/i2018-12664-5 (2018).

[73] S. Goriely, P. Dimitriou, M. Wiedeking, T. Belgya, R. Firestone, J. Kopecký, M. Krčíčka, V. Plujko, R. Schwengner, S. Siem, H. Utsunomiya, S. Hilaire, S. Péru, Y. S. Cho, D. M. Filipescu, N. Iwamoto,

T. Kawano, V. Varlamov, and R. Xu, The European Physical Journal A **55**, 10.1140/epja/i2019-12840-1 (2019).

[74] M. Honma, T. Otsuka, B. A. Brown, and T. Mizusaki, Physical Review C: Nuclear Physics **69**, 034335 (2004).

[75] K. Heyde, P. von Neumann-Cosel, and A. Richter, Rev. Mod. Phys. **82**, 2365 (2010).

[76] O. C. Gorton and C. W. Johnson, Phys. Rev. C **110**, 034305 (2024).

[77] C. W. Johnson and O. C. Gorton, Journal of Subatomic Particles and Cosmology **3**, 100061 (2025).

[78] O. C. Gorton, C. W. Johnson, and J. E. Escher, EPJ Web of Conferences **284**, 03013 (2023).

[79] Y. Iwata, N. Shimizu, T. Otsuka, Y. Utsuno, J. Menéndez, M. Honma, and T. Abe, Physical Review Letters **116**, 112502 (2016).

[80] Y. Utsuno, T. Otsuka, B. A. Brown, M. Honma, T. Mizusaki, and N. Shimizu, Physical Review C: Nuclear Physics **86**, 051301 (2012).

[81] C. W. Johnson and A. Keller, Centroids of nuclear shell-model hamiltonians, with optimization of energy-based truncation schemes (2025).

[82] M. Horoi, B. A. Brown, and V. Zelevinsky, Physical Review C: Nuclear Physics **50**, R2274 (1994).

[83] L. F. Jiao, Z. H. Sun, Z. X. Xu, F. R. Xu, and C. Qi, Physical Review C: Nuclear Physics **90**, 024306 (2014).

[84] J. Blomqvist and A. Molinari, Nuclear Physics A **106**, 545 (1968).

[85] D. Gloeckner and R. Lawson, Physics Letters B **53**, 313–318 (1974).

[86] O. C. Gorton and K. Kravvaris, Phys. Rev. C **112**, 014302 (2025).